Electronic Supplementary Material (ESI) for Journal of Materials Chemistry A.

Supplementary information

Flexible Fiber-Shaped Lithium and Sodium-Ion Batteries with Exclusive Ion Transport Channels and Superior Pseudocapacitive Charge Storage

*Yalei Wang, Yuanchuan Zheng, Jiupeng Zhao, * and Yao Li, **

Dr. Y. Wang, Dr. Y. Zheng, Prof. Dr. J. Zhao.

MIIT Key Laboratory of Critical Materials Technology for New Energy Conversion and Storage, School of Chemistry and Chemical Engineering, Harbin Institute of Technology, Harbin 150001, China.

Email: jpzhao@hit.edu.cn

Prof. Dr. Y. Li.

Center for Composite Materials and Structure, Harbin Institute of Technology, 150001, Harbin, China.

Email: yaoli@hit.edu.cn

Experimental Section

Materials: Cesium carbonate (Cs_2CO_3) and tungsten trioxide (WO_3) were purchased from Aladdin Bio-Chem Technology Co., Ltd. Tetrabutylammonium hydroxide (TBAOH) was purchased from Macklin Biochemical Co., Ltd. Graphite flakes were purchased from Sigma-Aldrich. All other chemicals were purchased from Sinopharm Chemical Reagent Co. Ltd. All the chemicals were analytical reagent grade and used without further purification.

Preparation of 2D Tungstate and GO LCs Colloids: Tungstate LCs colloid was fabricated from layered tungstate crystals by cation exchange exfoliation, as follows. The layered tungstate crystals were synthesized by protocol documented previously [1]. Cs_2CO_3 and WO_3 were mixed at a molar ratio of 4:11 in Pt crucible and heated at 1173 K for 5 h under air atmosphere. The obtained crystals were ground less than 75 μm and then immersed in 12M HCl solution for 2 days at room temperature to promote proton exchange, occurring a color change from dark green to white. And then, the suspension should be filtered and washed with deionized water to remove the excess HCl. After dried in air for 2 to 3 days, the resulting protonated crystals (for example, 0.8 g) were reacted with 100 ml of an aqueous solution including 0.0056 mol dm^{-3} TBAOH for 0.5 h followed by filtration and washing with deionized water until pH=7. Finally, the crystals should be dispersed in deionized water and shaken intermittently for about 8 h, then the tungstate LCs colloid was obtained with milky textures. The GO LCs colloid was synthesized from natural graphite flakes by a modified Hummers method reported previously [2]. In the pre-oxidation step, 40 mL concentrated sulphuric acid (H_2SO_4) was added into a 500 mL flask and then heated to 353 K. The potassium persulfate ($K_2S_2O_8$, 8.4 g) and phosphorus pentoxide (P_2O_5, 8.4 g) were added step by step gradually, and then the natural graphite flakes (10 g) was added slowly. After that, the mixture should keep at 353 K for 4.5 h under stirring. After cooling to room temperature, the mixture was diluted with deionized water and left overnight. Finally, the mixture was filtered by vacuum, washed with deionized water, and dried in air at room temperature. In the oxidation step, the pre-oxidation sample was added into a 1500 mL flask (containing 230 mL concentrated H_2SO_4) under continuous stirring at 273 K. Then potassium permanganate ($KMnO_4$, 60 g) was added slowly, and the temperature should keep below 283 K. Subsequently, mixture was heated to 308 K and stirred for 2 h, and then diluted with 500 mL deionized water, stirring for 2 h. Then an additional deionized water (1500 mL) was added and followed by dropwise addition of 30% hydrogen peroxide solution (H_2O_2, 25 mL). After setting undisturbed for 4 days, the clear supernatant was decanted, and the precipitate was repeatedly washed with water, 1M HCl solution and water successively until the pH=7. Finally, after mass production of GO nanosheets by ultrasonic exfoliation, removal of possible impurities and concentration by centrifugation, the GO LCs colloid was obtained.

Preparation of Tungstate/rGO Fiber: The 2D tungstate and GO LCs colloids were mixed homogeneously at mass ratio of 9: 1 and preloaded into a syringe pump as spinning dope. The tungstate/GO fiber was obtained when the mixed LCs colloid injected into a rotating coagulation bath (0.8 wt% chitosan in 4 wt% acetic acid solution), which should be soaked in the coagulation bath for over 15 min before the washing step and then dried under axial tension. The tungstate/rGO fiber was achieved after the chemical reduction of dried tungstate/GO fiber by hydroiodic acid at 90℃ for 4 h. After washing and drying, the average linear mass density of the tungstate/rGO fiber was 0.28-0.33 mg cm^{-1}.

Materials Characterizations: The POM observations were carried out on Leica DM4P polarization microscopy. The SEM images were taken on FEI HELIOS NanoLab 600i field-emission SEM system. The TEM/HRTEM images and SAED were taken on JEOL JEM-2100 Electron Microscope. The ultrathin sections of tungstate/rGO fiber were obtained by Leica EM UC7. The AFM images were taken on Bruker Dimension Fastscan. The TGA analysis was carried out on Netzsch STA449F3 under the air atmosphere. The Raman spectroscopy was collected on RENISHAW inVia-Reflex with laser of 532 nm. The XPS analysis was performed with Thermo Fisher ESCLAB 250Xi using Al Kα X-rays as excitation source. The tensile property was measured by SANS testing machine CMT-C102. The XRD data were collected by PANalytical Empyrean diffractometer using Cu Kα1 radiation ($\lambda = 0.1541$ nm) at 40 kV. The Zeta potential analysis was carried out on Malvern Zetasizer Nano ZS analyzer.

Electrochemical Measurements: The fiber-shaped battery was assembled in a heat shrink tubing under the argon atmosphere in a Mikrouna glove box. The tungstate/rGO fiber with an effective length of 8 cm was used as the working electrode, and the lithium and sodium wires positioned in parallel were utilized as the counter electrode for fiber-shaped LIBs and SIBs, respectively. One end of the tungstate fiber and lithium/sodium wire were connected with the copper wires by conductive silver adhesive and the manually cut Celgard 2400 and glass fiber membrane (GF/D, Whatman) were placed between them to prevent possible short circuit for fiber-shaped LIBs and SIBs, respectively. Before the heat shrinkable packaging, the $LiPF_6$ (1M) in ethylene carbonate and diethyl carbonate (1:1, by volume) and the $NaClO_4$ (1M) in ethylene carbonate and propylene carbonate (1:1, by volume) were injected into the tube as the electrolyte for fiber-shaped LIBs and SIBs, respectively. The cyclic voltammetry curves were collected on a CH Instruments 660E electrochemical workstation and the galvanostatic charge/discharge curves were recorded on a Land battery test system (LAND CT2001A) at room temperature.

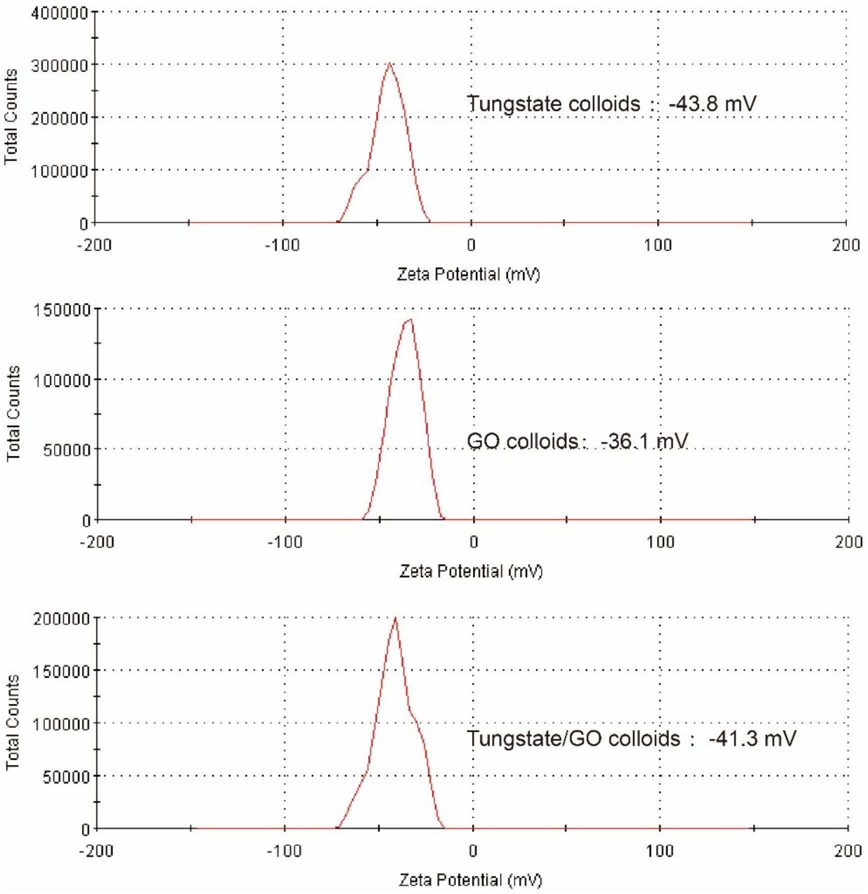

Figure S1. The Zeta potential for tungstate, GO, and mixed tungstate/GO liquid crystals colloids, which clearly signals the negative surface charge of the nanosheets.

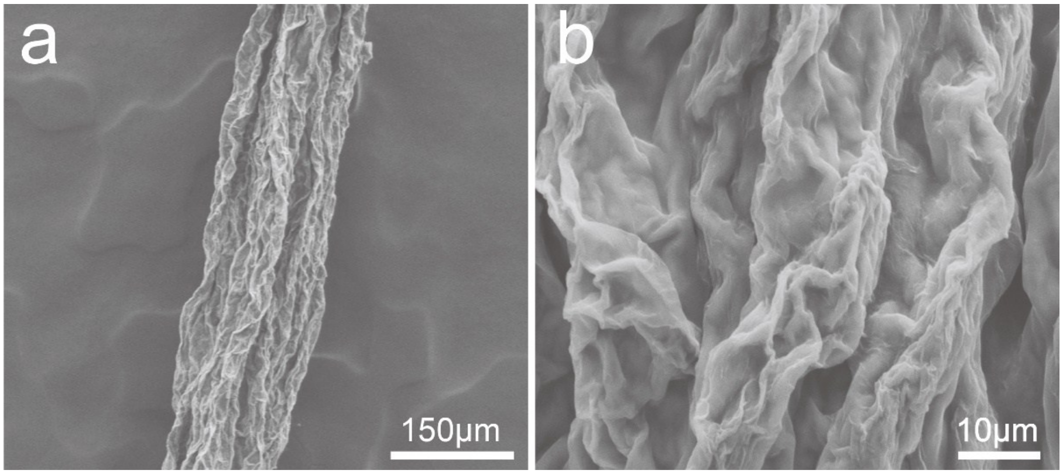

Figure S2. SEM images of tungstate/GO fiber. (**a, b**) SEM images of tungstate/GO fiber under different magnification.

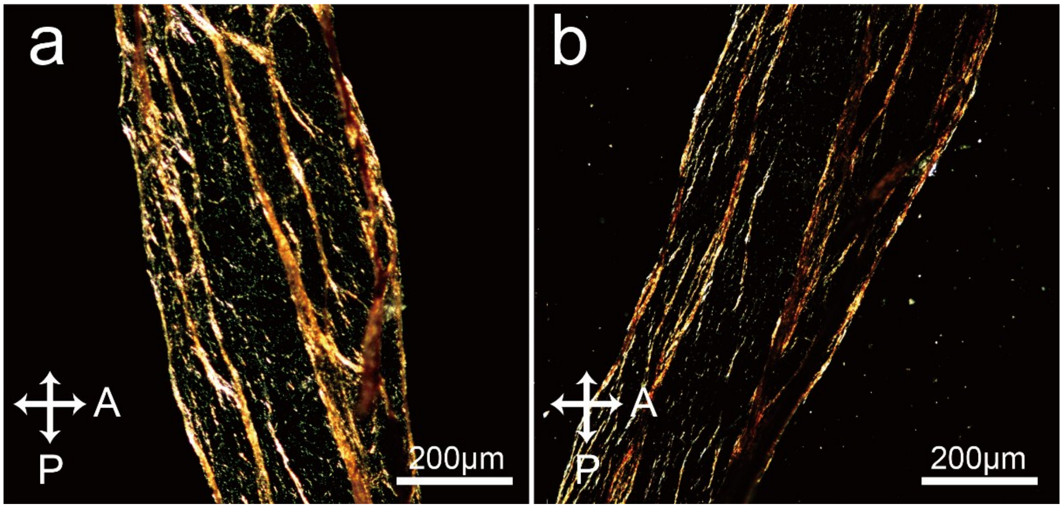

Figure S3. POM images for the tungstate/GO and tungstate/rGO fibers. (a) POM image of tungstate/GO fiber. (**b)** POM image of tungstate/rGO fiber.

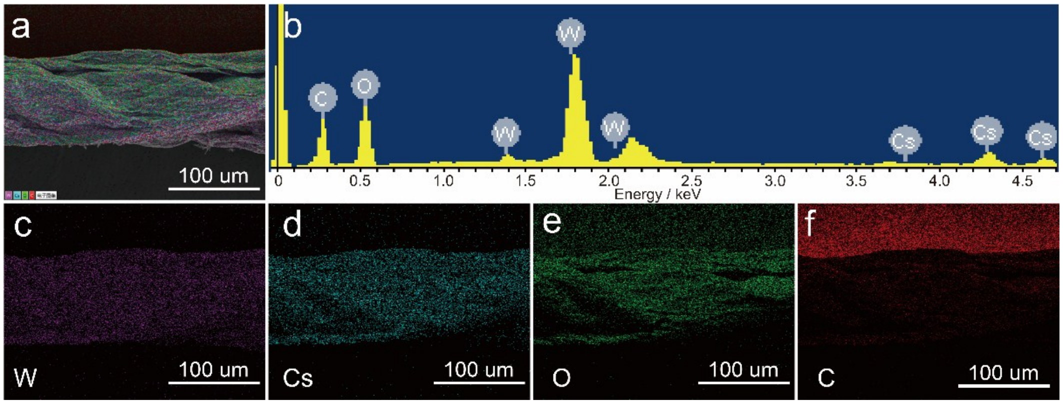

Figure S4. **EDS element analysis for tungstate/rGO fibers. (a)** Elements distribution for tungstate/rGO fiber. (**b)** EDS spectra for tungstate/rGO fiber. (**c-f)** EDS mapping of W-element, Cs-element, O-element, and C-element for tungstate/rGO fiber, respectively.

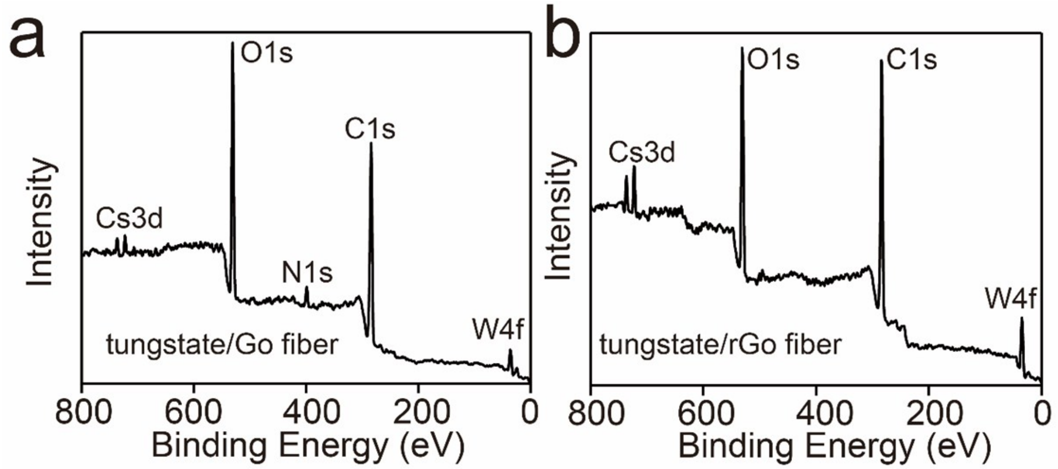

Figure S5. XPS survey spectrum for the tungstate/GO and tungstate/rGO fibers. (a) XPS survey spectrum for tungstate/GO fiber. (**b)** XPS survey spectrum for tungstate/rGO fiber. The N1s peak is disappeared after hydroiodic acid reduction, evidencing the removal of chitosan in tungstate/rGO fiber.

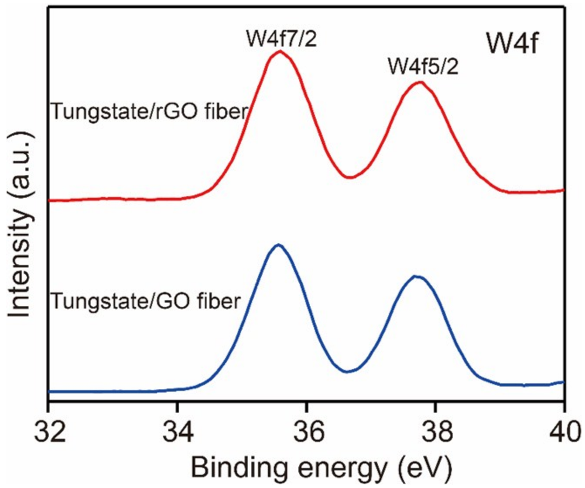

Figure S6. High-resolution XPS spectrum of W4f for tungstate/GO and tungstate/rGO fibers.

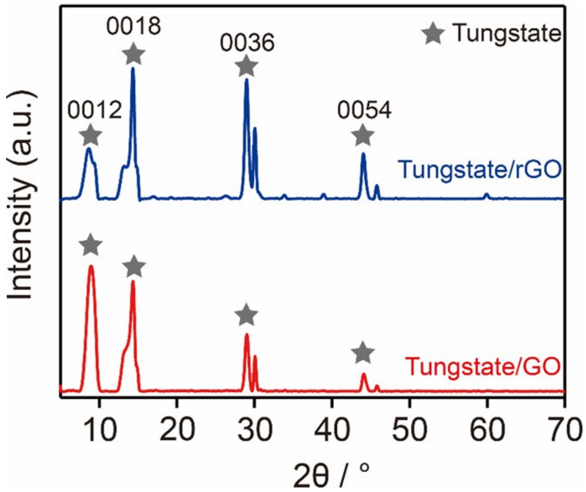

Figure S7. XRD pattern for the tungstate/GO and tungstate/rGO fibers.

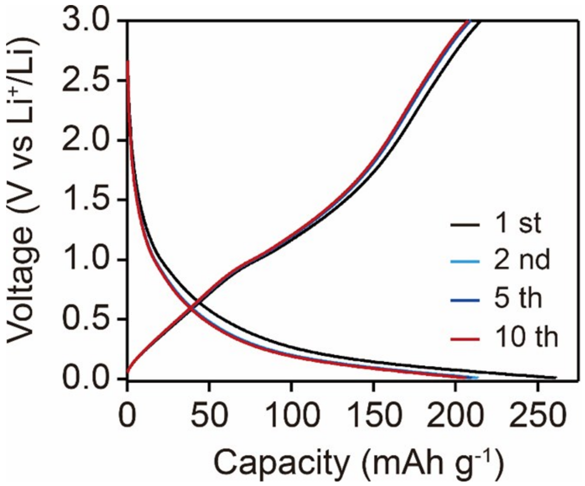

Figure S8. Galvanostatic charge/discharge profiles of the 1st, 2nd, 5th, and 10th cycles for fiber-shaped LIBs.

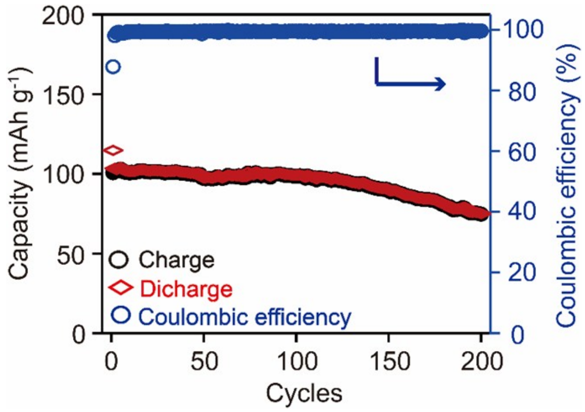

Figure S9. Electrochemical performances of pure tungstate for LIB. The electrochemical tests of pure tungstate were carried out by coin cell CR2032, using carbon black powders as conductive additive.

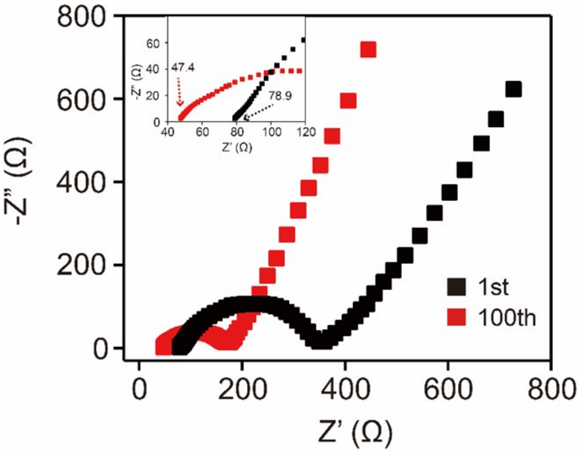

Figure S10. Nyquist plots measured for fiber-shaped LIB under open-circuit conditions. Inset: enlarged area of the high-frequency region with impedance values ranging between 40 and 120 Ω.

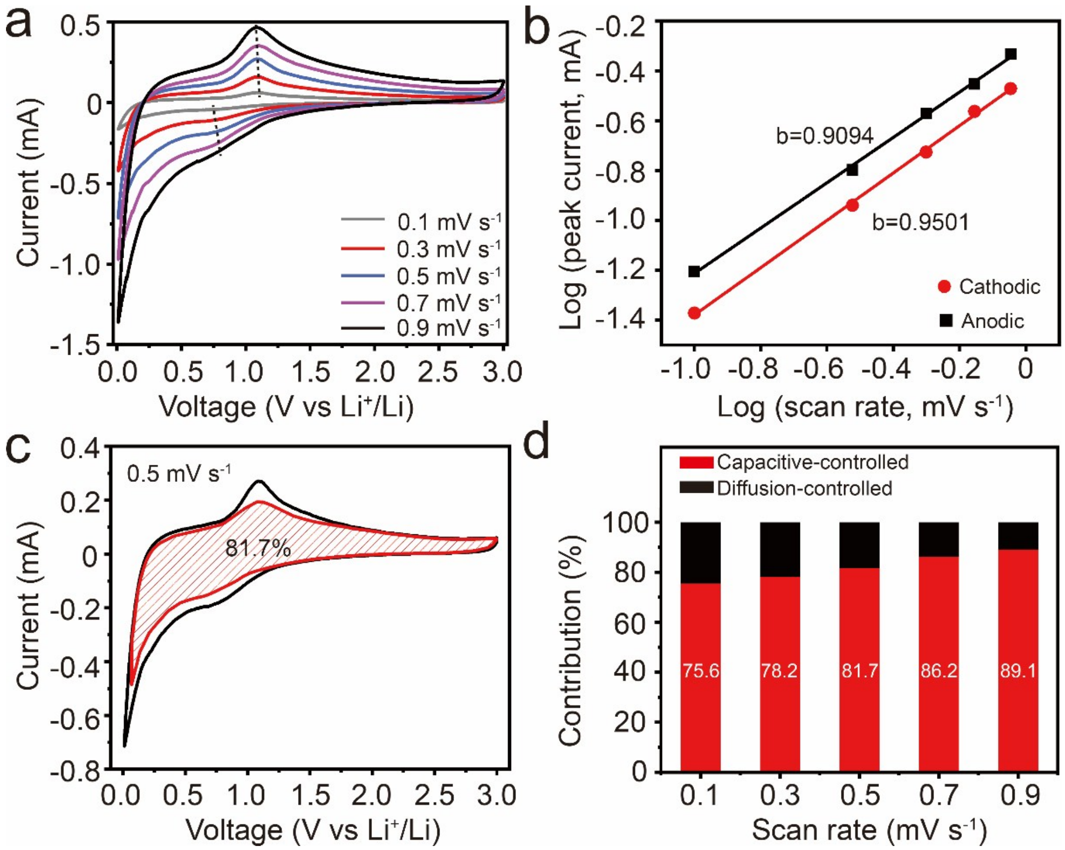

Figure S11. Kinetic analysis of the Li-ion storage mechanism in fiber-shaped LIBs. (a) CV curves at different scan rates from 0.1 to 0.9 mV s^{-1}. (**b)** Determination of the b-value by utilizing the power-law relationship between peak current and scan rate. (**c**), Capacitive-controlled (red) contribution to charge storage at 0.5 mV s^{-1}. (**d)** Contribution ratio of capacitive-controlled (red) and diffusion-controlled (black) capacities at different scan rates.

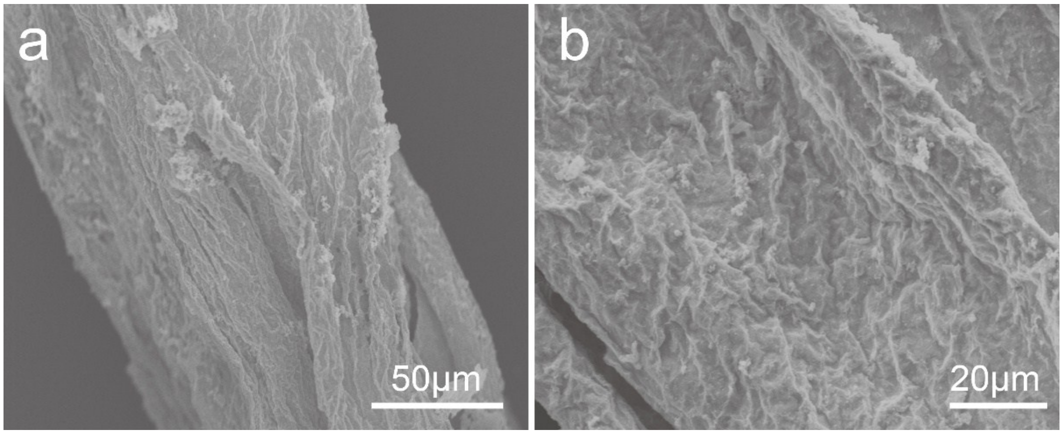

Figure S12. SEM images of the fiber electrode after 200 bending cycles for fiber-shaped LIBs. (a, b) SEM images of fiber electrode after 200 bending cycles. No obvious structural change and no substantial damage are observed.

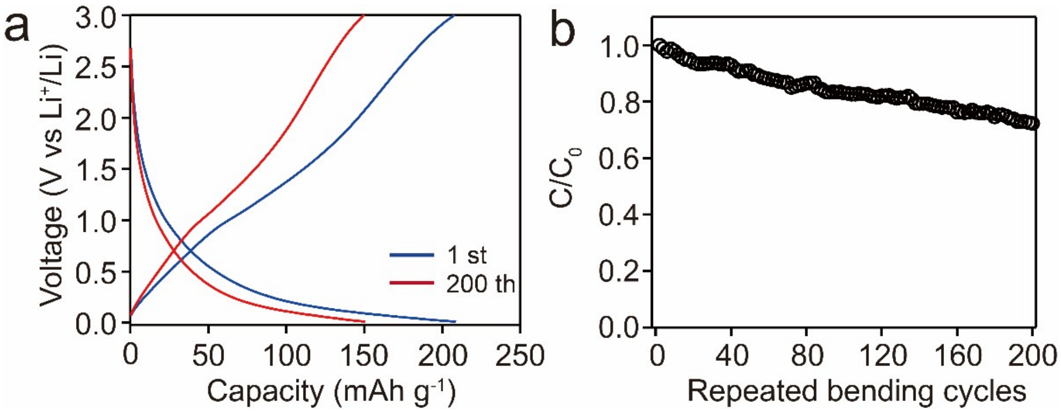

Figure S13. The life of fiber-shaped LIB under repeated bending. (a) Galvanostatic charge/discharge profiles of the 1st and 200th cycles for fiber-shaped LIBs under repeated bending. **(b)** The capacity retention for the fiber-shaped LIB under repeated bending.

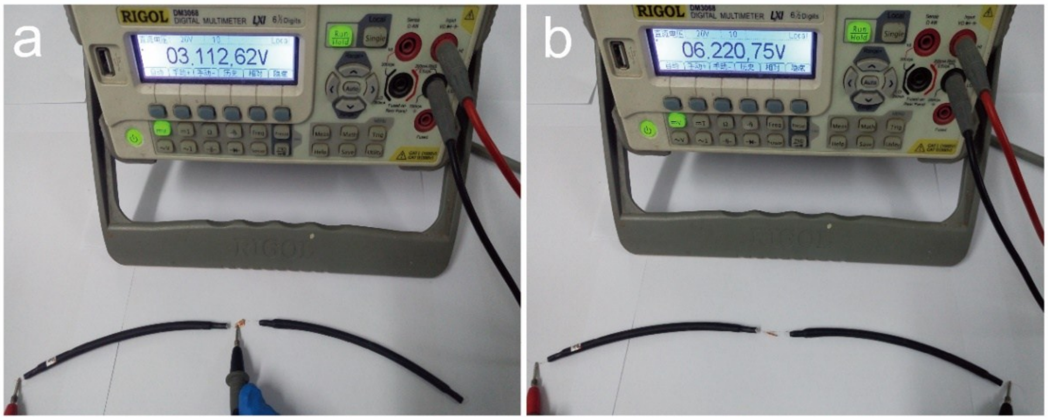

Figure S14. **Voltage outputs of the fiber-shaped LIBs. (a),** Photographs of the operating voltage for single fiber battery. (**b)** Photographs of the operating voltage for two fiber batteries in series

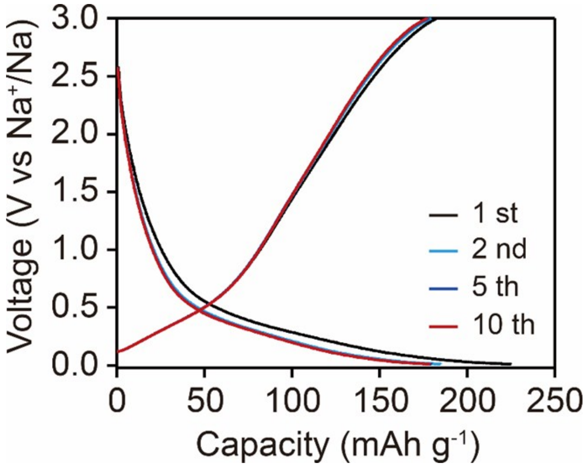

Figure S15. Galvanostatic charge/discharge profiles for the 1st, 2nd, 5th, and 10th cycles in fiber-shaped SIB.

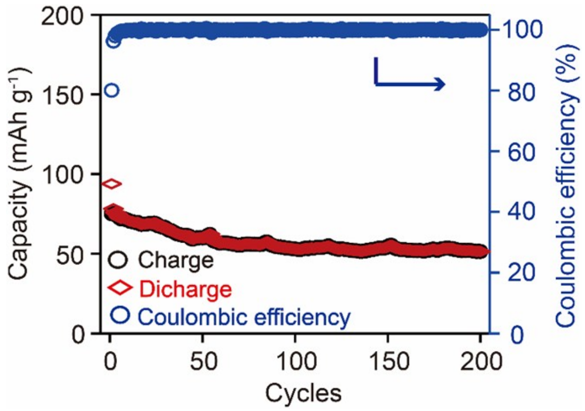

Figure S16. Electrochemical performances of pure tungstate for SIB. The electrochemical tests of pure tungstate were carried out by coin cell CR2032, using carbon black powders as conductive additive.

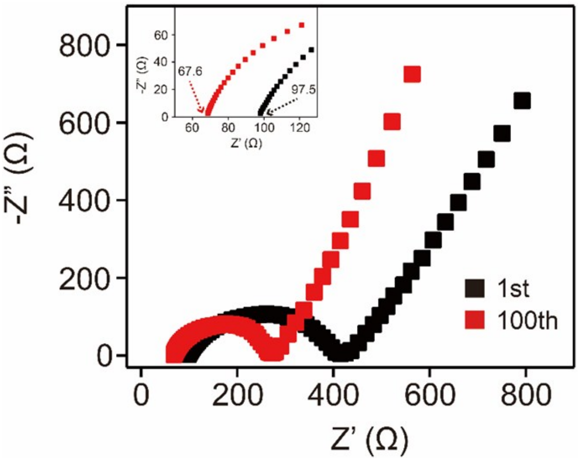

Figure S17. Nyquist plots measured for fiber-shaped SIB under open-circuit conditions. Inset: enlarged area of the high-frequency region with impedance values ranging between 50 and 130 Ω.

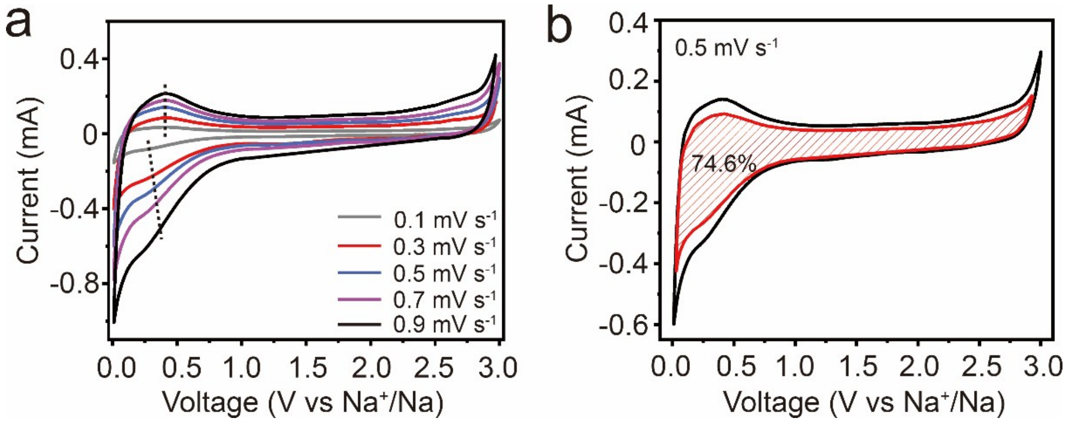

Figure S18. Kinetic analysis of the Na-ion storage mechanism in fiber-shaped SIBs. (a) CV curves at different scan rates from 0.1 to 0.9 mV s^{-1}. (**b)** Capacitive-controlled (red) contribution to charge storage at 0.5 mV s^{-1}.

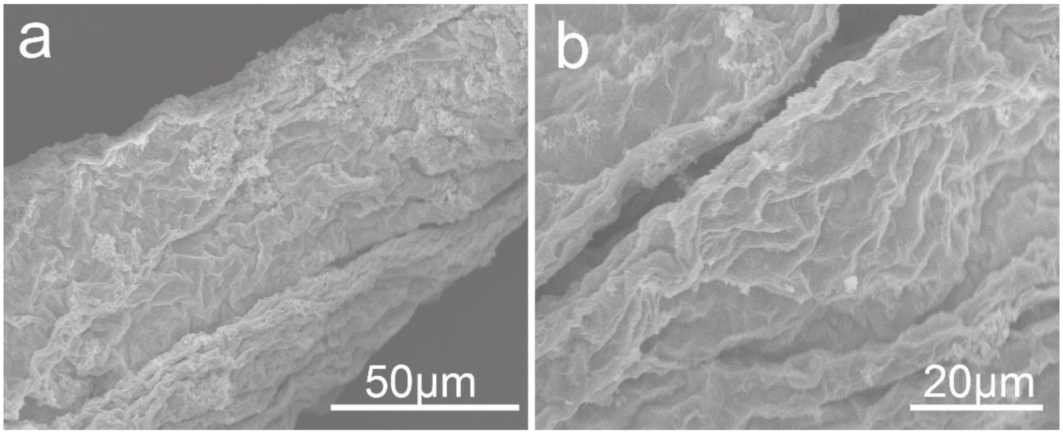

Figure S19. SEM images of the fiber electrode after 200 bending cycles for fiber-shaped SIBs. (a, b) SEM images of fiber electrode after 200 bending cycles. No obvious structural change and no substantial damage are observed.

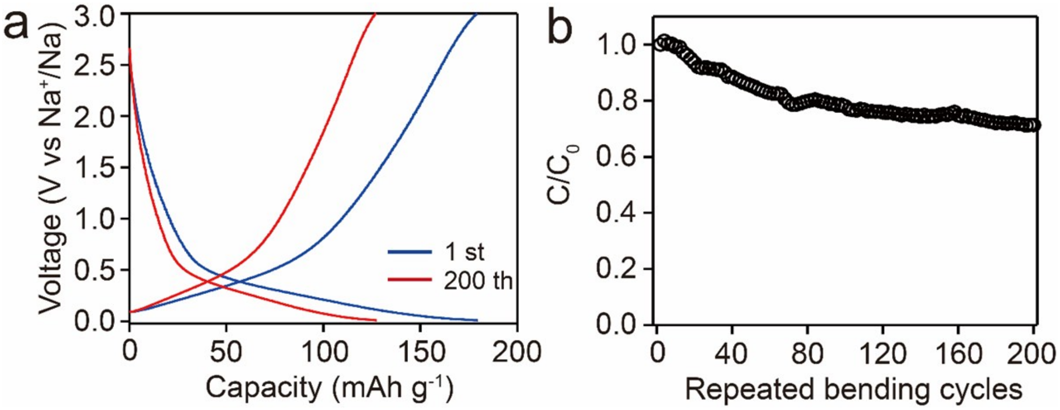

Figure S20. The life of fiber-shaped SIB under repeated bending. (a) Galvanostatic charge/discharge profiles of the 1st and 200th cycles for fiber-shaped SIBs under repeated bending. **(b)** The capacity retention for the fiber-shaped SIB under repeated bending.

Table S1. Comparison of 1D fiber-shaped LIBs and SIBs batteries.

Type	**Cathode**	**Anode**	**Capacity**	**Long-term Cycling Retention**	**Bending Cycling Retention**	**Ref.**
LIBs	Tungstate/rGO	Li wire	137.9 mAh g^{-1} (0.520 mA)	81.1% (1000th)	77% (200th)	**This work**
	$LiCoO_2$/Al wire	Ni-Sn/Cu wire	1 mAh cm^{-1} (0.1 C)	80% (8th)	No	[3]
	MnO_2/CNT	Li wire	218 mAh g^{-1} (0.0005 mA)	-	No	[4]
	Si/CNT	Li wire	1670 mAh g^{-1} (1 A g^{-1})	32% (100th)	No	[5]
	$LiMn_2O_4$/CNT	Si/CNT	106.5 mAh g^{-1} (1 C)	87% (100th)	No	[6]
	$LiMn_2O_4$/CNT	$Li_4Ti_5O_{12}$/CNT	70 mAh g^{-1} (0.05 mA)	85% (100th)	No	[7]
	$LiMn_2O_4$/CNT	$Li_4Ti_5O_{12}$/CNT	92.4 mAh g^{-1} (0.1 mA cm^{-1})	92.1% (100th)	No	[8]
	$LiMn_2O_4$/CNT	$Li_4Ti_5O_{12}$/CNT	91.3 mAh g^{-1} (0.1 mA cm^{-1})	78% (100th)	No	[9]
	MoS_2/CNT	Li wire	1298 mAh g^{-1} (0.2 A g^{-1})	96% (100th)	No	[10]
	$LiFePO_4$/CNT	$Li_4Ti_5O_{12}$/CNT	110 mAh g^{-1} (50 mA g^{-1})	81% (30th)	No	[11]
	Titania/rGO	Li wire	168 mAh g^{-1} (0.0085 mA)	80% (100th)	No	[12]
	MoS_2/CNT	Li-ZnO/CNT	1176mAh g^{-1} (50 mA g^{-1})	96% (100th)	No	[13]
SIBs	Tungstate/rGO	Na wire	102.2 mAh g^{-1} (0.520 mA)	86% (1000th)	78.8% (200th)	**This work**
	$Na_{0.44}MnO_2$ / Cu wire	NGQDs-WS_2- 3DCF/Cu wire	59.8 mAh g^{-1} (50 mA g^{-1})	97% (100th)	No	[14]
	NiS_2/PCF	Na foil	363 mAh g^{-1} (5 C)	75.8% (5000th)	No	[15]
	PB@GO@NCT	Na foil	110 mAh g^{-1} (0.5 C)	76% (120th)	~58% (60th)	[16]
	Titania/rGO-CNTs	Na wire	111 mAh g^{-1} (17 mA g^{-1})	60.3% (2000th)	~60% (800th)	[17]

Reference

[1] K. Fukuda, K. Akatsuka, Y. Ebina, R. Ma, K. Takada, I. Nakai, T. Sasaki, ACS Nano 2008, 2, 1689.

[2] Z. Xu, C. Gao, ACS Nano2011 5(4), 2908.

[3] Y. H. Kwon, S. W. Woo, H. R. Jung, H. K. Yu, K. Kim, B. H. Oh, S. Ahn, S. Y. Lee, S. W. Song, J. Cho, H. C. Shin, J. Y. Kim, Adv. Mater. 2012, 24, 5192.

[4] J. Ren, L. Li, C. Chen, X. Chen, Z. Cai, L. Qiu, Y. Wang, X. Zhu, H. Peng, Adv. Mater. 2013, 25, 1155.

[5] H. Lin, W. Weng, J. Ren, L. Qiu, Z. Zhang, P. Chen, X. Chen, J. Deng, Y. Wang, H. Peng, Adv. Mater. 2014, 26, 1217.

[6] W. Weng, Q. Sun, Y. Zhang, H. Lin, J. Ren, X. Lu, M. Wang, H. Peng, Nano Lett. 2014, 14, 3432.

[7] J. Ren, Y. Zhang, W. Bai, X. Chen, Z. Zhang, X. Fang, W. Weng, Y. Wang, H. Peng, Angew. Chem. Int. Ed. 2014, 126, 7998.

[8] Y. Zhang, W. Bai, X. Cheng, J. Ren, W. Weng, P. Chen, X. Fang, Z. Zhang, H. Peng, Angew. Chem. Int. Ed. 2014, 53, 14564.

[9] Y. Zhang, W. Bai, J. Ren, W. Weng, H. Lin, Z. Zhang, H. Peng, J. Mater. Chem. A. 2014, 2, 11054.

[10] Y. Luo, Y. Zhang, Y. Zhao, X. Fang, J. Ren, W. Weng, Y. Jiang, H. Sun, B. Wang, X. Cheng, H. Peng, J. Mater. Chem. A. 2015, 3, 17553.

[11] Y. Wang, C. Chen, H. Xie, T. Gao, Y. Yao, G. Pastel, X. Han, Y. Li, J. Zhao, K. Fu, L. Hu, Adv. Funct. Mater. 2017, 27, 1703140.

[12] T. Hoshide, Y. Zheng, J. Hou, Z. Wang, Q. Li, Z. Zhao, R. Ma, T. Sasaki, F. Geng, Nano Lett. 2017, 17, 3543.

[13] X. Wang, Z. Pan, J. Yang, Z. Lyu, Y. Zhong, G. Zhou, Y. Qiu, Y. Zhang, J. Wang, W. Li, Energy Storage Mater. 2019.

[14] Y. Wang, D. Kong, S. Huang, Y. Shi, M. Ding, Y. V. Lim., T. Xu., F. Chen, X. Li, H. Y. Yang, J. Mater. Chem. A. 2018, 6, 10813.

[15] Q. Chen, S. Sun, T. Zhai, M. Yang, X. Zhao, H. Xia, Adv. Energy Mater. 2018, 8, 1800054.

[16] Y. H. Zhu, S. Yuan, D. Bao, Y. B. Yin, H. X. Zhong, X. B. Zhang, J. M. Yan, Q. Jiang, Adv Mater 2017, 29, 1603719.

[17] Y. Zhou, K. Jiang, Z. Zhao, Q. Li, R. Ma, T. Sasaki, F. Geng, Energy Stor. Mater. 2019.